

TABLE 2. Mean (and median) properties of  $B_{gq}$  groups

Property	$B_{gq} > 350$		$B_{gq} < 350$		Difference (high $B_{gq}$ wrt low $B_{gq}$ )
	mean	(median)	mean	(median)	
$B_{gq}$	833	(792)	37	(0)	(defining cut)
$z$	0.55	(0.58)	0.52	(0.51)	—
$m_v$	17.6	(17.0)	17.6	(17.2)	—
$M_v$	-23.7	(-24.3)	-23.5	(-23.7)	0.2 (0.5)
Source type (1-4)	3.5	(4)	2.7	(3)	$\sim 1$
Size (kpc)	162	(134)	142	(135)	(types 3,4 only)
			100	(53)	all types - larger?
Bend angle ( $^\circ$ )	8	(6)	16	(9)	less bent?
Lobe length ratio	0.72	(0.72)	0.71	(0.65)	—
Source complexity (1-5)	2.8	(3)	3.0	(3)	—
# other sources	0.67	(0)	0.71	(0)	(1.6 in X-ray clusters)
$\alpha_{core}$	-0.08	(-0.12)	-0.12	(-0.03)	—
Power 6cm C	25.4	(25.4)	25.6	(25.6)	-0.2 (-0.2)
(W/Hz) 20cm C	25.4	(25.2)	25.7	(25.5)	-0.3 (-0.3)
6cm L1	25.6	(25.7)	25.1	(24.9)	0.4 (0.8)
6cm L2	25.2	(25.3)	24.9	(24.9)	0.3 (0.4)
20cm L1	25.9	(26.0)	25.5	(25.5)	0.4 (0.5)
20cm L2	25.6	(25.6)	25.4	(25.4)	0.2 (0.2)
mean Lobe	25.6	(25.7)	25.2	(25.2)	0.4 (0.5)

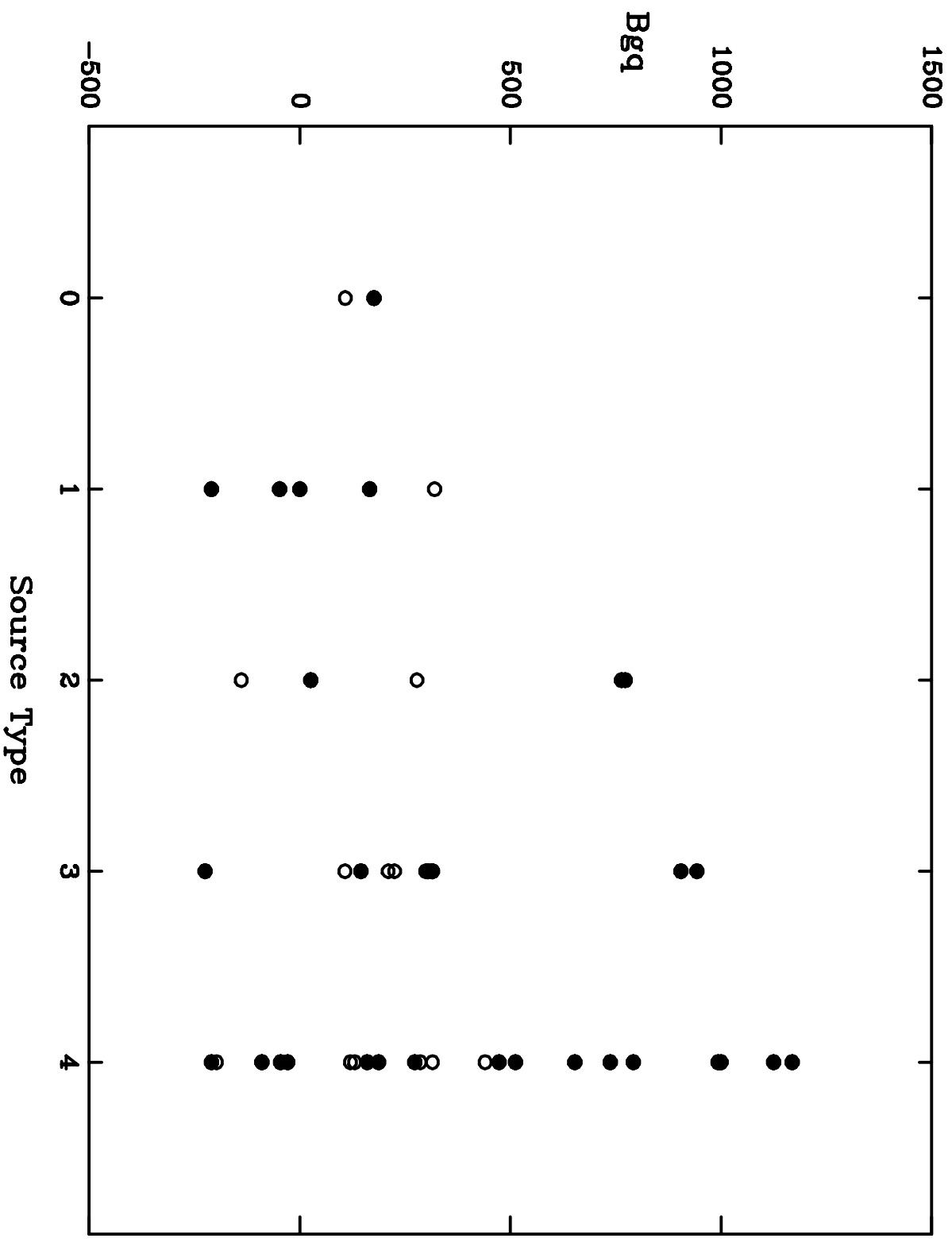
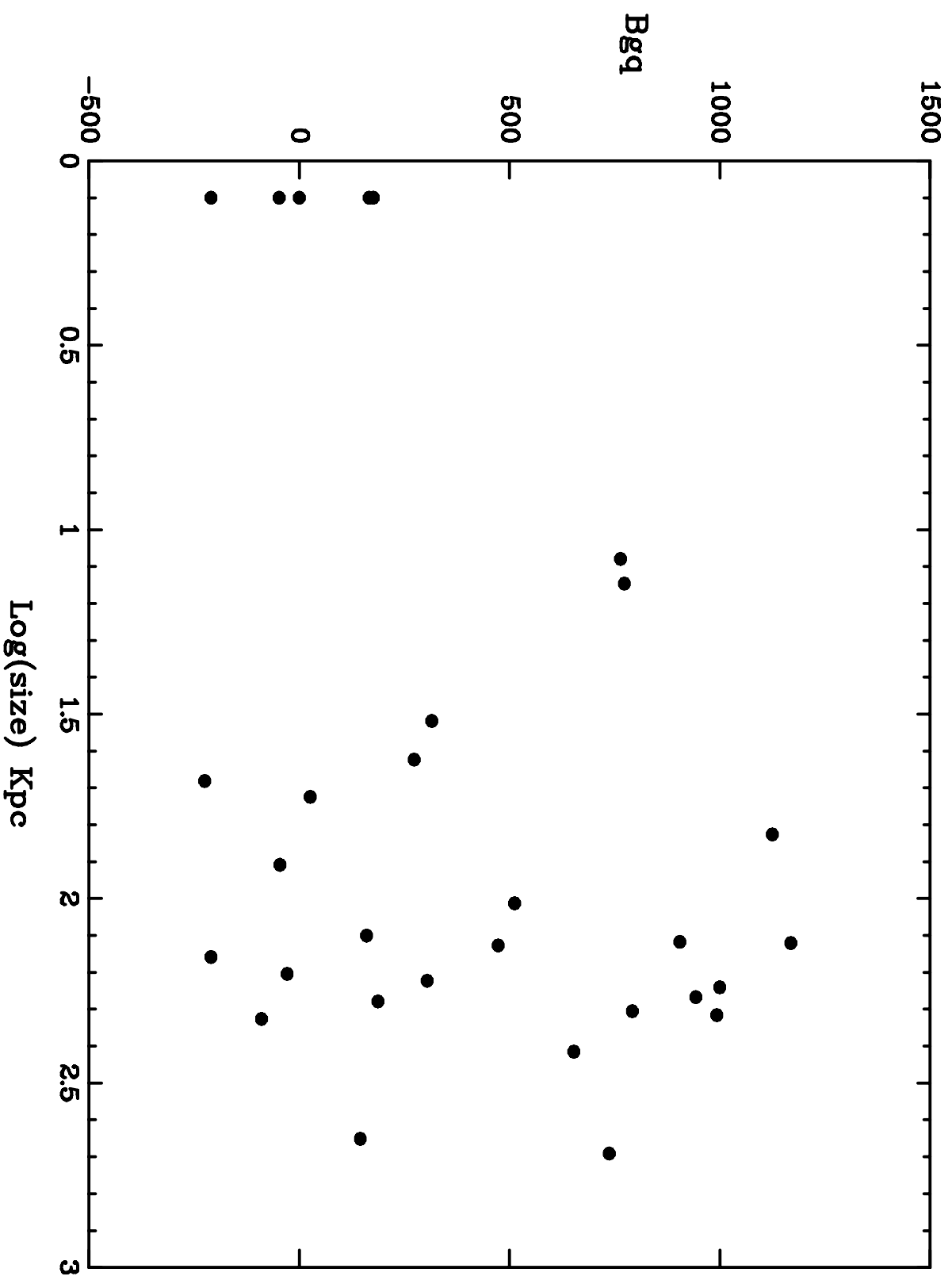
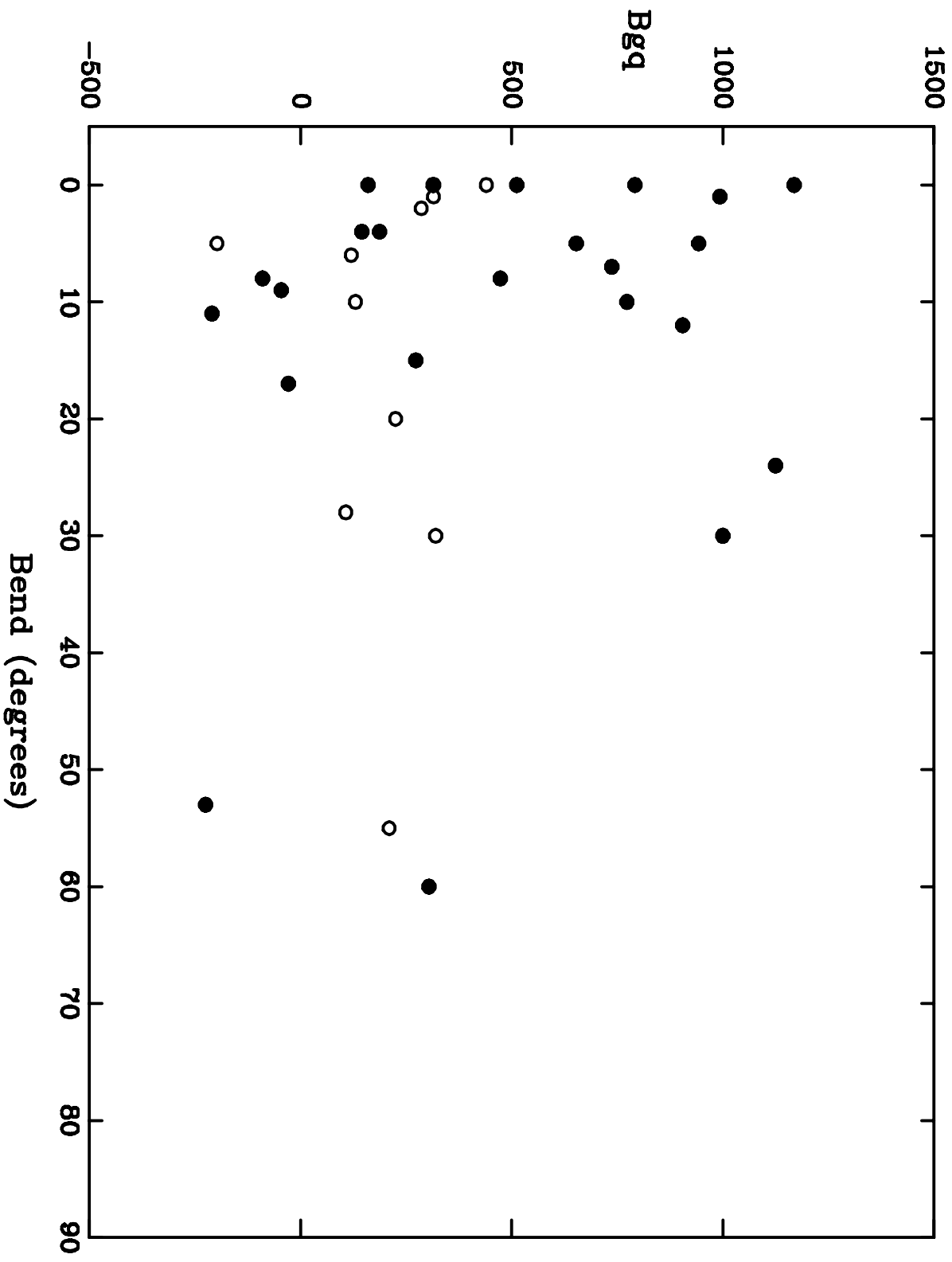
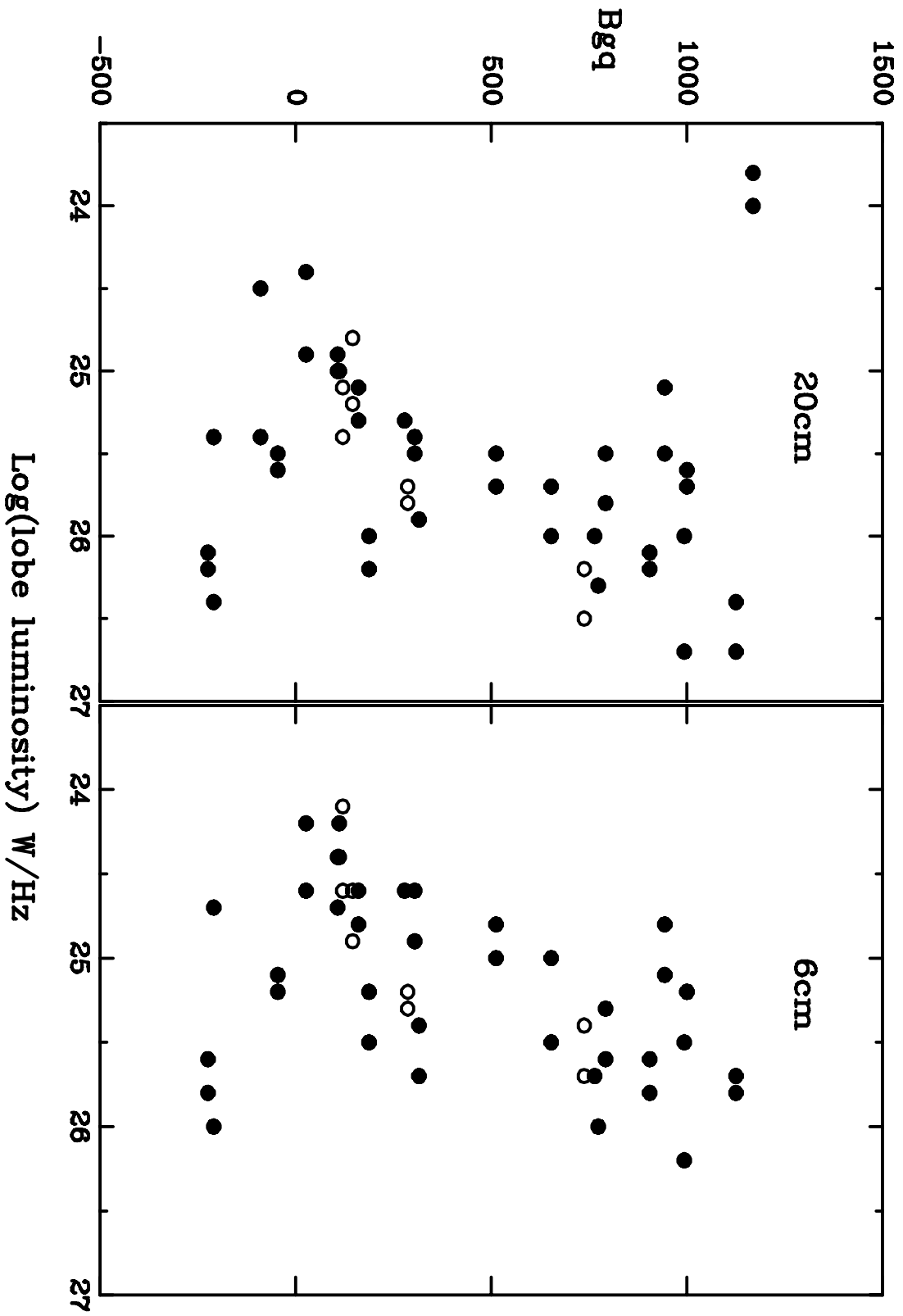


TABLE 3. Cluster field source counts

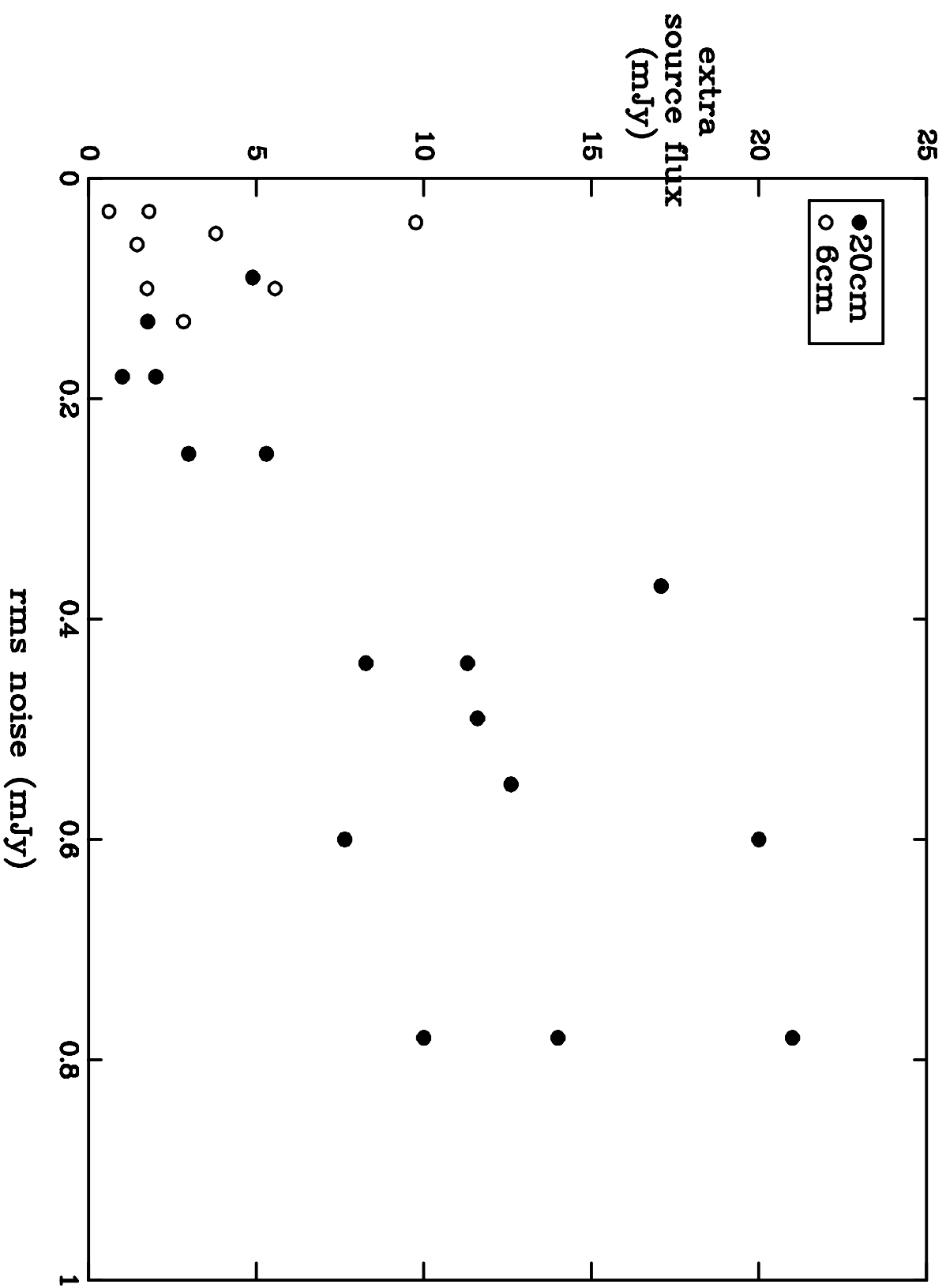
QSO cluster	Rich cluster (mean of 4)	A2390 (exceptional)	Mean ratio rich/QSO	
			incl central source	w/o central source
1.4 (>4mJy)	2.7	4	2.1	4.5
1.6 (>1.5mJy)	2.8	6	2.1	3.6

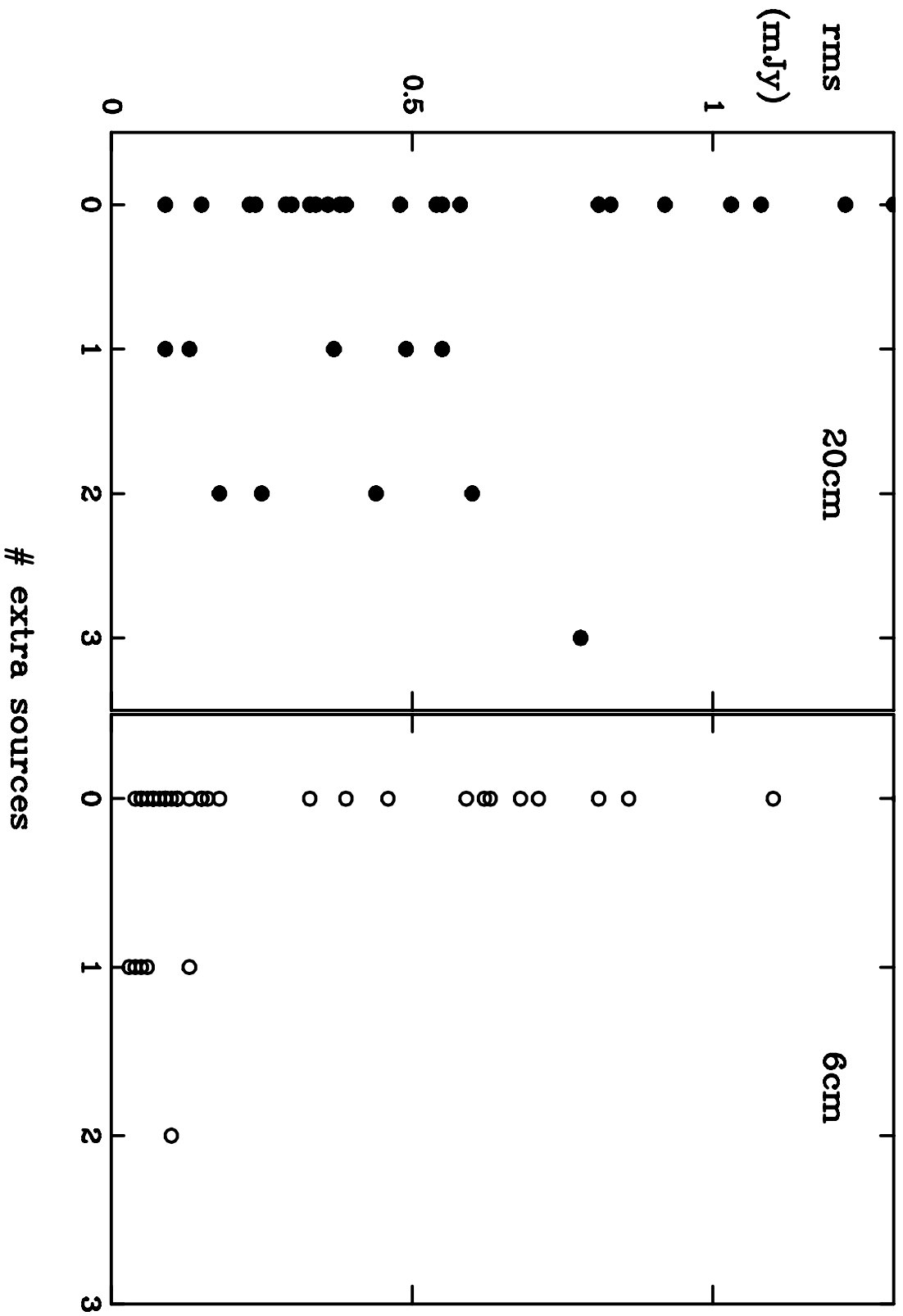


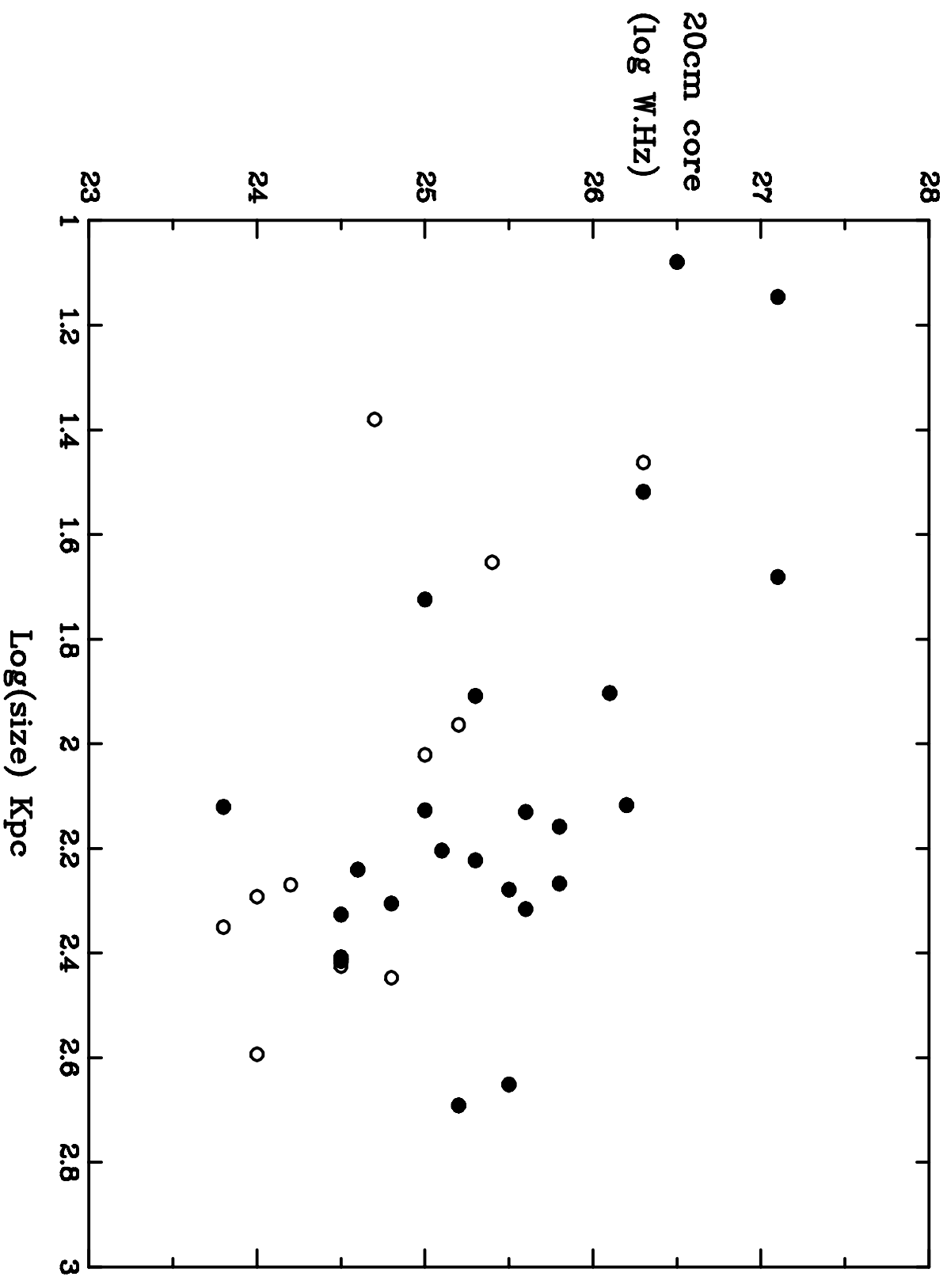


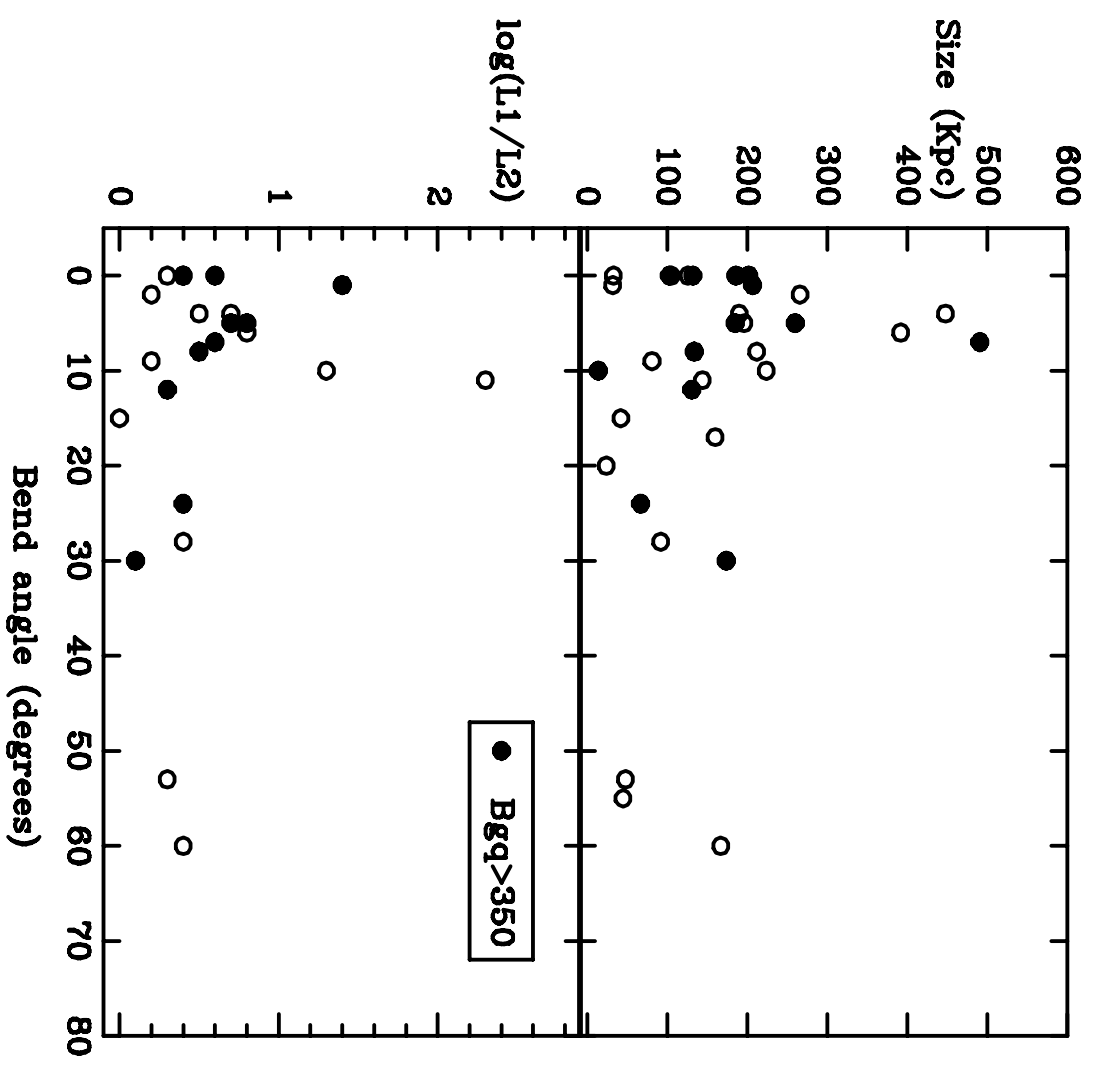












# QUASAR RADIO STRUCTURE IN CLUSTER ENVIRONMENTS

J.B.Hutchings

Dominion Astrophysical Observatory, National Research Council of Canada  
5071 W. Saanich Rd., Victoria, B.C. V8X 4M6, Canada

A.C.Gower

Dept of Physics and Astronomy, University of Victoria  
P.O Box 1700, Victoria, B.C, Canada

S.Ryneveld and A.Dewey

Dominion Astrophysical Observatory, National Research Council of Canada  
5071 W. Saanich Rd., Victoria, B.C. V8X 4M6, Canada

Received \_\_\_\_\_; accepted \_\_\_\_\_

## ABSTRACT

VLA<sup>1</sup> B-configuration snapshots have been obtained at 6cm and 20cm of 43 radio quasars with a range of known galaxy cluster environments. The radio sources are characterised by measures of morphology, flux, and size. These are studied as a function of cluster density, characterised by published  $B_{gq}$  numbers. We find no strong dependence of radio source properties on this measure of cluster density. We find  $\sim 2\sigma$  evidence that sources in higher cluster densities have more lobe-dominated morphology with higher lobe luminosities and lower core luminosities. The 7 unresolved sources are found in low density clusters, as are the most bent sources. We find that QSO clusters have fewer other radio sources within a radius of 3 arcminutes than do the central galaxies of a sample of rich X-ray selected clusters.

---

<sup>1</sup>The Very Large Array is a part of the National Radio Astronomy Observatory, which is operated by Associated Universities Inc, under contract with the NSF

## 1. Introduction

We have obtained radio images of 43 QSOs of redshift 0.7 or less with a range of known galaxy environments from optical studies. The program was planned to study the connection between radio source properties and the galaxy cluster density around the QSO. The cluster density of the QSOs is measured by the  $B_{gq}$  number derived from the galaxy companion data largely published separately by Yee and Ellingson (1993 and references therein). These numbers have units of  $\text{Mpc}^{1.77}$ . We have optical images of some of the clusters, but do not yet have a uniform dataset that allows us to measure other cluster properties, such as size, or the location of the QSO within the cluster.

The radio observations were made in the B-configuration of the VLA, in December 1991, taking  $\sim 5$  minute snapshots of 50 sources at 6cm and 20cm, interspersed with calibration sources, and determining the flux density scale using 3C48 and 3C138. The images were self-calibrated where possible. The synthesised beam in the final images is  $\sim 4$  arcsec at 20cm and  $\sim 1.3$  arcsec at 6cm. The largest-scale structure fully determined in the B-configuration observations is  $\sim 100$  arcsec at 20cm, and  $\sim 35$  arcsec at 6cm, and care was taken when discussing the radio structure of QSOs with angular sizes comparable with or larger than these values. We have also used the A-configuration maps of Price et al (1993) and Gower and Hutchings (1984) of 10 of the sample QSOs, and also of 11 more QSOs with  $B_{gq}$  measures, for which we have A-configuration measures by Hutchings, Price and Gower (1988), or Gower and Hutchings (1984). This gives us a total sample of 54 QSOs with radio data, of which we have  $B_{gq}$  values for 45.

A similar investigation has been published by Rector, Stocke, and Ellingson (1995), based on published radio maps of QSOs with known  $B_{gq}$  values. Since the  $B_{gq}$  value is the common parameter, there is an overlap of 16 objects in our specifically observed sample, and another 9 for which we had earlier maps, within their sample of 30 objects. We discuss

the comparison of conclusions at the end of this paper.

The maps and related details will be published separately. The list and measures relevant to this paper are listed in Table 1. The sources were characterised by measures of flux density, morphology, size, and shape, also shown in Table 1. The bend angles are defined by the core and hot-spots in the lobes and are usually well-defined. The source types are defined in the Table 1 footnotes, and are based on whether one or two lobes are present, and the relative flux densities of core and lobes at 20cm. The classification depends on the resolution of small-scale structure (hence redshift), and dynamic range where the lobe flux per beam area is very low. The system is the same as that used in papers on QSO and radio galaxy structure from A-configuration maps, as referred to above. Many of the quantities in the A-configuration maps are taken from the measures in the references given. We have also listed a source ‘complexity’ measure assigned independently by two of us from visual inspection of the maps. This is meant mainly to quantify non-symmetry which is not measured by source type and bend.

We also noted where other faint radio sources were detected in the field, to investigate the presence of other cluster sources, and also to study the possible effect of the cluster on background sources. The map dynamic range was usually in the range 500 to 1200 (peak flux density to RMS noise). Values outside this range were found in exceptionally weak sources where thermal noise dominated at 0.1 mJy at 20cm and 0.04 mJy at 6cm, or strong sources where dynamic range dominated ( $\sim 2000$  for peak fluxes above 2Jy: 4 sources have noise above 1mJy at 6cm and 3 have noise above 2mJy at 20cm).



## 2. Cluster environment

The distribution of the  $B_{gq}$  values indicates a spread of values about zero, together with a distribution of higher values (see Figure 1). From this distribution, we consider values below 350 as representing the statistical spread around the mean galaxy-galaxy correlation amplitude - i.e. not significantly clustered. Values above 350 are taken to represent the significantly clustered environments. Figure 2 shows the distribution of  $B_{gq}$  with redshift: in order to use a subset matched in redshift for high and low  $B_{gq}$ , we select QSOs with redshift higher than 0.4. Table 2 shows mean and median values of properties in this matched sample of 32, divided into the high and low  $B_{gq}$  groups. In measuring the lobe fluxes, we also rejected 2 more sources with sizes larger than  $85''$ , which may have missing flux. (These lie one in each group, and in fact do not alter our results. We also retain these 2 objects in the other radio source measures, which are not affected by missing flux.)

Table 2 suggests the following differences: 1) The high  $B_{gq}$  group has a more lobe-dominated mean type (see Figure 3): *all* compact sources are in low  $B_{gq}$  environments). 2) High  $B_{gq}$  environment sources have higher lobe luminosities, by a factor 2-3 (see Figure 6). 3) High  $B_{gq}$  sources have lower core luminosities (by a factor  $<2$ ). There is a strong relationship between size and core luminosity (Figure 9 and Neff and Hutchings 1990, first noted by Hutchings Price and Gower 1988), which relates this with the next point. 4) High  $B_{gq}$  sources have larger source size, particularly when the unresolved sources are included (Figure 4). 5) High  $B_{gq}$  sources have less bent sources (Figure 5.).

We do not quote uncertainties in Table 2 as most of the quantities do not have gaussian distributions, and differences between properties in the two groups cannot be quantified simply in terms of their spread. To test significance we have done K-S tests, which indicate that points 1 - 5 above are significant at the  $2\sigma$  to  $3\sigma$  level. Also, there are significant continuous correlations with  $B_{gq}$  for the luminosities (Figure 6). However, the lobe length

ratio, source complexity, and core spectral index, show no dependence on  $B_{gg}$ .

These results are somewhat counter to the expectation that a more dense cluster environment would bend or inhibit extended source growth. This could indicate that in higher density clusters, the IGM is less chaotic or dense, or that galaxy density is not related to the state of the IGM at these redshifts.

### 3. Source counts

In several of the B-configuration maps, one or two other sources were detected. These are unresolved and typically faint, but all those listed in Table 1 are  $12\sigma$  or more above their RMS map noise levels. It is of interest to study these extra sources to understand whether they are in the QSO cluster, or background sources, with possible lensing by the cluster. The detection of these sources will be affected by the map noise (usually determined by the main source flux density), the bandwidth smearing with distance from the map centre, and the source flux density itself. The primary beam attenuation at 20cm is negligible over the small field radii considered here. If the sources are in the cluster then the limiting detectable luminosity will also depend on the cluster redshift. We look at these different effects in turn.

Overall, a total of 22 extra sources are detected in the 43 fields in the 20cm maps. At 20cm, the density of sources per unit sky area around the map centre is constant out to radius  $\sim 3.2$  arcmin, and then falls rapidly, with only five lying outside that. The fall-off may begin at radius 2.6 arcmin, but by less than 30%. This is just where we expect the bandwidth smearing to become noticeable. Thus, we exclude the sources beyond 3.2 arcmin. The number and flux level of extra sources is not correlated with the cluster redshift, and so we apply no redshift filter or correction.

In the 6cm maps, we detect 8 extra sources, of which only one is not seen at 20cm. Some of the sources are marginally resolved at 6cm, but none have definite structure. The one 6cm source not seen at 20cm may be a component of another nearby seen at both frequencies, but otherwise there is no reason to suppose that different sources in a field are related to each other.

At 20cm, the number of sources detected per field is about the same for all map noise levels below 0.8 mJy (Figure 7). However, the lowest flux density of detected sources appears to rise, as expected, for noise levels above 0.3 mJy (see Figure 8). The 6cm noise levels and flux densities are lower, and extra sources are detected only in maps of noise 0.15 mJy and less. In Figure 8 we can see that at 20cm we detect 6 ( $<3.2$ arcmin) sources in 10 eligible fields with noise  $<0.3$  mJy, and 16 sources in 25 eligible fields with noise  $<0.8$  mJy. These fractions are very similar (0.60 and 0.64), because the low noise fields have no sources above 10mJy and only one above 6mJy (perhaps the result of small number statistics). Our result is thus that the average QSO cluster contains  $\sim 0.4$  extra sources within 3.2 arcmin, to a 20cm flux limit of  $\sim 4$  mJy. To a limit of 1mJy this number is  $\sim 0.6$  per field. In the 6cm maps the fraction is 0.3 per field, with a lower flux density limit, but very small number statistics. In addition, the primary beam response varies significantly over this field size at 6cm, so that some sources at large radii may fall below the detection limit.

We looked for counterparts in the known galaxy companions to the QSOs, but almost all the sources lie outside the radius of the distribution of known companions. The few closer ones are not coincident with the (incomplete) list of known cluster members. The total flux of all background sources at 20cm expected in this area of sky, is  $\sim 17$ mJy, which is more than the mean extra source flux we detect (6.1mJy average from the 25 0.8mJy-noise eligible fields). Thus, the extra source flux does not exceed that expected from background sources.

As a comparison, we looked for the extra sources detected in our maps of very rich (X-ray selected) clusters, from the CNOC program (paper in preparation). (This program was undertaken by the Canadian Network for Observational Cosmology and is described e.g. by Yee, Ellingson and Carlberg 1996.) These clusters do not have strong central sources, but in all 5 cases, the central cD galaxy was detected as one of the strongest sources. We thus counted extra sources around the cD galaxies, with the same flux density and area limits as in our QSO clusters. The rich cluster maps have lower noise and detection limits than those of the QSO program. The numbers are summarized in Table 3.

The comparisons in Table 3 show that the rich clusters contain on average more sources than the QSO clusters. However, their total flux density does not exceed the expected background. The rich clusters have slightly lower mean redshift than the QSO clusters. This has implications for source luminosity limits if they are cluster members, which we discuss in the last section. In the central regions of the rich clusters, we have deep optical images, in which we may identify the radio sources. So far, we have only looked at the exceptionally rich A2390 cluster, and only one of the 6 of the central sources corresponds with an optical source to limits 6 magnitudes fainter than the cD galaxy (Abraham et al 1996).

The mean  $B_{gq}$  of the CNOC clusters is 1400, compared with 300 for the QSO sample, although some of the QSO clusters have  $B_{gq}$  near to 1000. There is no correlation between  $B_{gq}$  and number of sources in the QSO sample, so that it may be that X-ray selection finds clusters with properties not measured by  $B_{gq}$ . In any case, the preliminary evidence is that one rich X-ray selected cluster has an enhanced population of radio sources near its centre, which is either associated with optically very faint objects, or represents background source fluxes which are enhanced, perhaps by a gravitational lensing effect.

#### 4. Other radio source properties

The new B-configuration data generally show the same results as our earlier work using A-configuration maps of over 250 radio quasars of redshifts up to 3.5. These are discussed in papers by Neff and Hutchings (1990), and Lister, Hutchings and Gower (1994), and references therein.

There is a correlation between core luminosity and source size (Figure 9), but not with lobe luminosity. We previously discussed this in terms of source evolution in which a strong core source fades as the lobes grow. The relation between bend angle and size (Figure 10) is similar to that of Lister et al (1994). There is no correlation between bend angle and either core or lobe luminosity. The more bent sources are also more complex on a more widespread level, and the most complex sources are generally small. This suggests that sources which are complex have been affected by a nuclear event or by a dense medium, or are significantly foreshortened by projection. Finally, the most bent sources have lobes of nearly equal luminosity, while those with most uneven lobes are not bent.

#### 5. Discussion

Rector et al (1995) have published tables and analysis similar to ours on the QSO source structure. Their conclusions are in agreement with ours, but there are some detailed differences we should note. The individual source sizes and bend angles differ in detail, presumably as a result of map noise, dynamic range, resolution, and occasionally differences in interpreting complex sources. An example of the latter is 0903+169, where we give a bend of  $30^\circ$  compared with their value of  $58^\circ$  (which they flag as uncertain). In this instance there are several compact knots near the 20cm map centre, and the bend angle measured depends on which is assumed to be the core. We believe we have chosen correctly

by adopting the one which is brightest in our 6cm map. Some of their bend measures depend on the optical position when the radio core was not visible: our measures are based on a homogenous set of maps obtained by ourselves, and only radio source features are used. Thus, our database is more complete and uniform. Similarly, the flux measures are all measured from our maps, and we regard them as more complete and homogenous than those quoted by Rector et al. In some cases, there are significant differences between their values and ours, which look like cases where the core or lobe fluxes were difficult to measure or may have suffered from poor dynamic range. We also note that the linear sizes used by Rector et al, correspond to  $H_0=50$ , and not 100 as stated in their paper. Thus, the sizes we quote (for  $H_0=100$ ,  $q_0=0.5$ ) are about a factor two smaller than theirs. Finally, we note that they have chosen to split high and low  $B_{gq}$  at 500, which corresponds to a certain Abell richness, while we have chosen 350 on the basis of the numbers in our sample. Again, the difference is not very significant, and a matter of choice.

The overall conclusion we reach is similar to that of Rector et al: that there are no strong correlations with  $B_{gq}$ . The significance level of the differences we have highlighted between high and low  $B_{gq}$  sources are at the 2 to  $3\sigma$  level, either by K-S tests between the two groups, or by the correlation with  $B_{gq}$  as a parameter.

The lack of strong correspondence with  $B_{gq}$  suggests that this quantity does not measure the IGM well. There have been recent reports of correspondence between radio and hot gas (X-ray) structure, in low redshift clusters such as Virgo and Perseus (e.g. Brinkman 1996 and Owen 1996). If QSOs are at the centre of their clusters, they may have little movement through the cluster, and any IGM movement may be infall (i.e. not transverse to the radio structure). It would be of interest to look for radio structure correlations with the QSO position within the cluster, and the velocity structure of the clusters. Ellingson, Green and Yee (1991) have published velocity studies of a few of the QSO clusters in the

sample, but there are too few measurements to make any comparisons. They do note that the cluster velocity dispersions are fairly low, and that they see no significant differences in the relative velocities of companion galaxies between radio-loud and radio-quiet QSOs.

We have counts of sources in the QSO cluster fields, which are lower than those found in very rich clusters at comparable redshifts. We have not yet been able to determine whether these extra sources are associated with cluster galaxies. If they are cluster members, the mean difference in redshift corresponds to a difference of a factor close to 2 in limiting luminosity. If they are background sources, there may be implications of gravitational lensing. We are pursuing these studies with optical investigations.

Finally, we note that our new data add to and reinforce our results from earlier studies of QSO radio structure in the distribution of bend angle and core flux with apparent size. Thus, QSOs in cluster environments do not appear to have large differences from the behaviour of QSOs selected without knowledge of their environment.

We thank Erica Ellingson and Travis Rector for useful discussions. The new radio maps were made in collaboration with Erica Ellingson and will be published separately.

## REFERENCES

- Abraham R.G. et al 1996 ApJ (in press)
- Brinkman W. 1996 in IAU Symposium 175 (in press)
- Ellingson E., Green R.F., Yee H.K.C., 1991, ApJ, 378, 476
- Gower A.C. and Hutchings J.B. 1984, AJ, 89, 1658
- Hutchings J.B., Price R. and Gower A.C., 1988, ApJ, 329, 122
- Lister M.L., Hutchings J.B., and Gower A.C., 1994, ApJ, 427, 125
- Neff S.G. and Hutchings J.B. 1990, AJ, 100, 1441
- Owen F.N. 1996 in IAU Symposium 175 (in press)
- Price R., Gower A.C., Hutchings J.B., Talon S., Duncan D., Ross G., 1993, ApJS, 86, 365
- Rector T.A., Stocke J.T., Ellingson E., 1995, AJ, 110, 1492
- Yee H.K.C. and Ellingson E., 1993, ApJ, 411, 43
- Yee H.K.C., Ellingson E., and Carlberg R., 1996, ApJS, 102, 269



Captions to figures

Fig. 1.— Distribution of  $B_{gq}$  values of whole sample, and the subsample matched in redshift.

Fig. 2.— Redshift distribution of  $B_{gq}$  values. Solid symbols are matched  $z>0.4$  subset, and large symbols are sources larger than  $85''$ , which may have missing lobe flux.

Fig. 3.—  $B_{gq}$  values as a function of source type (see Table 1 footnote). Open symbols sources with  $z<0.4$ . High  $B_{gq}$  environments have no small or unresolved sources.

Fig. 4.—  $B_{gq}$  values for  $z>0.4$  subset as a function of source size. Five unresolved or just-resolved sources have arbitrarily low size values.

Fig. 5.—  $B_{gq}$  values with bend angle. Solid symbols are from  $z>0.4$  subset.

Fig. 6.—  $B_{gq}$  with lobe luminosities. Open symbols represent four sources with sizes larger than  $85''$ , which may have missing flux.

Fig. 7.— Number of extra sources detected within 3.2 arcmin, showing the map RMS noise lower limits of 0.8 and 0.2 mJy at 20cm and 6cm, respectively.

Fig. 8.— Flux densities of extra sources as a function of map RMS noise.

Fig. 9.— Core luminosity with source size. Solid symbols are from  $z>0.4$  subset.

Fig. 10.— Source size and lobe luminosity ratio with bend angle. Trends like these are modelled with orientation by Lister et al (1994).

TABLE 1. QSO cluster data

Name	z	C	Flux (mJy)			20cm			6cm			P (W/Hz)			Size Kpc	$\alpha_c$	Type <sup>a</sup>	Bend ( <sup>o</sup> )	length ratio	Cx
			6cm L1	L2	C	L1	L2	C	L1	L2	C	20cm L1	L2	"						
Measures from B-configuration maps																				
0042+101	0.583	16	12	1.2	16	127	60	24.4	24.3	23.3	24.5	25.4	25.1	60	226	0.0	3	5	0.9	2
0044+030	0.624	16	20	7.4	52	40	12	24.6	24.2	25	24.9	24.4	23.9	12	46	-0.9	2	—	—	—
0110+318	0.603	308	95	—	540	—	—	25.8	25.3	—	26	—	—	—	—	-0.5	1	—	—	—
0113-118	0.672	2063	50	—	—	—	—	26.7	25.1	—	—	—	—	—	—	—	2	—	—	—
0115+027	0.672	136	140	118	—	800	500	25.5	25.6	25.5	—	26.3	26.1	13	51	—	3	12	0.68	3
0119+041	0.637	1330	75	—	926	920	60	26.5	25.2	—	26.3	26.3	25.1	—	—	0.3	1	—	—	—
0130+242	0.457	—	—	—	33	260	30	—	—	—	24.5	25.4	24.5	53	181	—	4	8	0.82	—
0134+329*	0.367	5574	—	—	15424	—	—	26.6	—	—	27	—	—	—	—	-0.8	0	—	—	—
0222+000	0.523	89	—	—	253	—	—	25	—	—	25.6	—	—	—	—	-0.9	0	—	—	—
0300-004	0.693	45	258	75	—	690	190	25.1	25.8	25.3	—	26.3	25.7	8	32	—	4	11	0.78	2
0349-146+	0.616	31	270	130	67	1600	800	24.8	25.7	25.4	25.2	26.5	26.2	117	449	-0.6	4	7	0.94	2
0403-132	0.571	2026	600	—	3854	—	—	26.5	26	—	26.8	—	—	—	—	-0.5	1	—	—	—
0405-123	0.574	784	350	205	847	830	750	26.1	25.8	25.6	26.2	26.2	26.1	32	120	-0.1	3	12	0.73	3
0742+318+	0.462	737	75	33	276	130	55	25.9	24.9	24.6	25.5	25.2	24.8	112	385	0.8	3	4	0.95	2
0805+578	0.438	24	95	61	—	460	305	24.4	25	24.8	—	25.7	25.5	27	93	—	4	0	0.96	3
0846+100*	0.366	5	34	25	10	150	150	23.5	24.4	24.2	23.8	25	25	64	197	—	4	10	0.71	3
0903+169	0.411	175	180	170	40	500	390	25.2	25.2	25.2	24.6	25.7	25.6	47	153	1.2	4	30	0.90	5
0928+008	0.505	378	11	—	253	—	—	25.7	24.2	—	25.5	—	—	—	—	0.3	1	—	—	—
1007+417	0.611	358	430	25	303	1200	130	25.9	26	24.7	25.8	26.4	25.4	32	122	0.1	4	11	0.57	3
1012+232	0.565	751	61	9	796	230	60	26.2	25	24.2	26.1	25.6	25	19	71	0.0	3	5	0.51	—
1012+488*+	0.385	4	55	15	11	300	155	23.5	24.6	24.1	24	25.4	25.1	109	344	-0.9	4	6	0.97	3
1048-090*	0.344	69	310	280	55	990	830	24.6	25.3	25.2	24.5	25.8	25.7	83	247	0.2	4	2	0.79	2
1049+489	0.478	—	—	—	5	8	5	—	—	—	23.8	24	23.8	33	115	—	4	0	0.27	2
1058+110	0.423	5	62	40	—	200	140	23.7	24.8	24.6	—	25.3	25.1	34	112	—	4	0	0.94	3
1103-006	0.426	151	152	136	227	430	330	25.2	25.2	25.1	25.3	25.6	25.5	22	73	-0.3	4	9	0.80	4
1104+167	0.634	399	52	30	268	140	60	25.9	25.1	24.8	25.8	25.5	25.1	41	159	0.3	3	5	0.93	4
1137+660	0.646	130	730	144	162	2200	480	25.5	26.2	25.5	25.6	26.7	26	44	171	-0.2	4	—	0.52	2
1156+631	0.594	19	160	60	15	540	250	24.6	25.5	25	24.5	26	25.7	59	224	0.2	4	5	0.70	3
1200-051*	0.381	420	30	25	384	70	—	25.5	24.4	24.3	25.5	24.7	—	—	—	0.1	1	30	0.91	3
1241+166	0.577	226	380	270	—	2700	1400	25.6	25.8	25.7	—	26.7	26.4	16	60	—	4	24	0.65	3
1253-055	0.538	9552	410	280	8090	1100	760	27.2	25.8	25.6	27.1	26.2	26.1	15	55	0.1	3	53	0.36	4
1305+069	0.602	18	180	90	32	350	170	24.6	25.6	25.3	24.8	25.8	25.5	47	179	-0.5	4	0	0.55	3
1352-104*	0.332	314	80	45	244	180	140	25.3	24.7	24.4	25.2	25.0	24.9	28	82	0.2	3	28	0.43	3
1510-089*	0.361	2054	60	—	2538	300	—	26.2	24.6	—	26.3	25.3	—	9	27	-0.2	2	—	—	—
1546+027	0.413	887	6	—	619	24	—	25.9	23.7	—	25.7	24.4	—	—	—	0.3	1	—	—	—
1548+114	0.436	194	80	40	233	310	230	25.3	24.9	24.6	25.3	25.5	25.4	44	147	-0.2	3	60	0.85	4
1618+177	0.555	132	210	105	210	1900	560	25.3	25.5	25.2	25.5	26.2	26	46	170	-0.4	4	4	0.62	4
1641+399	0.595	5144	500	—	6423	950	—	27	26	—	27.1	26.3	—	3	11	-0.2	2	10	0.65	—
2131-021	0.557	1672	150	—	1028	120	—	26.5	25.4	—	26.2	25.3	—	—	—	0.4	1	—	—	—

arXiv:astro-ph/9602100v1 [21 Feb 1996]

TABLE 1. (continued)

Name	z	C	Flux (mJy)			20cm			6cm			P (W/Hz)			Size Kpc	$\alpha_c$	Type <sup>a</sup>	Bend ( <sup>o</sup> )
			6cm L1	L2	C	L1	L2	C	6cm L1	L2	C	20cm L1	L2	”				
2142+110	0.55	300	10	—	233	50	—	25.7	24.2	—	25.6	24.9	—	34	125	0.2	2	—
2251+134	0.673	491	210	100	785:	340	340	26.1	25.7	25.4	26.3:	25.9	25.9	7	28	-0.4	3	0
2252+129	0.543	390	360	—	1865:	700	—	25.8	25.7	—	26.5:	26	—	3	11	-1.3	2	—
2318+049	0.622	592	30	—	515	65	—	26.1	24.8	—	26	25.1	—	—	—	0.1	1	—
Measures from A-configuration maps																		
0003+158	0.450	125	—	—	88	—	—	25.1	25.0	24.5	25.0	25.5	25.5	36	122	0.3	4	8
0137+012*	0.258	150	—	—	230	—	—	24.8	—	—	25	—	—	38	95	-0.4	3	0
1217+023*	0.240	320	—	—	220	—	—	25.0	—	—	24.8	—	—	105	251	0.3	3	—
1302-102*	0.286	1185	—	—	570	—	—	25.7	—	—	25.4	—	—	12	32	0.6	3	55
1545+210*	0.264	—	—	—	35	—	—	—	—	—	24.2	—	—	70	178	—	4	0
1704+608*	0.371	6	—	—	18	—	—	23.6	26.0	—	24.1	26.0	25.0	60	186	-0.9	4	5
2209+080	0.484	225	—	—	—	—	—	25.4	25.5	25.5	—	26.0	26.0	11	39	—	4	15
2247+140	0.235	1210	—	—	1870	—	—	25.6	—	—	25.8	—	—	1	2	-0.4	2	—
2251+113*	0.323	18	—	—	—	—	—	24.0	25.5	25.0	—	25.5	25.5	10	29	—	4	—
2305+187*	0.313	81	—	—	80	—	—	24.7	—	—	24.7	—	—	8	22	0.0	3	20
2314-116	0.549	91	—	—	81	—	—	25.2	24.5	—	25.1	25.5	25.5	60	221	0.1	4	17

Notes to Table 1.

\* Not included in matched  $z > 0.4$  sample + 3 sources with structure  $> 80''$  may have missing lobe flux

All quantities are for  $H_0=100$ ,  $q_0=0.5$

<sup>a</sup>0 = unresolved; 1 = extended core; 2 = core + 1 lobe; 3 = dominant core + 2 lobes; 4 = core and 2 stronger lobes

<sup>b</sup>Source ‘complexity’ increasing from 1 to 5

<sup>c</sup>Number of additional sources in field

<sup>d</sup>Units of Mpc<sup>1.77</sup>